

## POSSIBLE DETECTION OF A CYCLOTRON RESONANCE SCATTERING FEATURE IN THE X-RAY PULSAR 4U 1909+07

GAURAVA K. JAISAWAL<sup>1</sup>, SACHINDRA NAIK<sup>1</sup>, BISWAJIT PAUL<sup>2</sup>

*Draft version August 7, 2021*

### ABSTRACT

We present timing and broad-band spectral studies of the high mass X-ray binary pulsar 4U 1909+07 using data from *Suzaku* observation during 2010 November 2-3. The pulse period of the pulsar is estimated to be  $604.11 \pm 0.14$  s. Pulsations are seen in the X-ray light curve up to  $\sim 70$  keV. The pulse profile is found to be strongly energy-dependent: a complex, multi-peaked structure at low energy that becomes a simple single peak at higher energy. We found that the 1-70 keV pulse averaged continuum can be fitted by the sum of a black body and a partial covering Negative and Positive power-law with EXponential cutoff (NPEX) model. A weak iron fluorescence emission line at 6.4 keV was detected in the spectrum. An absorption like feature at  $\sim 44$  keV was clearly seen in the residue of the spectral fitting, independent of the continuum model adopted. To check the possible presence of a CRSF in the spectrum, we normalized the pulsar spectrum with the spectrum of the Crab Nebula. The resulting Crab ratio also showed a clear dip centered at  $\sim 44$  keV. We performed statistical tests on the residue of the spectral fitting and also on the Crab spectral ratio to determine the significance of the absorption like feature and identified it as a CRSF of the pulsar. We estimated the corresponding surface magnetic field of the pulsar to be  $3.8 \times 10^{12}$  Gauss.

*Subject headings:* X-rays: stars – neutron, pulsars – stars: individual – 4U 1909+07

### 1. INTRODUCTION

Accretion powered X-ray binary pulsars which were discovered in the early 70s (Giacconi et al. 1971), are among the brightest X-ray sources in sky. These binary systems consist of a neutron star with strong magnetic field ( $B \sim 10^{12}$  Gauss) and a supergiant or a Be star as optical companion. Mass transfer from the companion star to the neutron star takes place through Roche lobe overflow (in case of low mass X-ray binaries such as Her X-1, Reynolds et al. 1997) and/or capture of stellar wind (in high mass X-ray binary systems). The accreted matter is channeled towards the magnetic poles of the neutron star by its strong magnetic field forming accretion columns from where the gravitational energy of accreted matter is being dissipated in the form of X-rays. Most of accretion powered X-ray pulsars belong to the group of high-mass X-ray binary (HMXB) systems. Based on spectral and luminosity class of companion stars, the HMXBs are further classified into two subgroups such as (i) Supergiant X-ray binary (SGXB) systems and (ii) Be/X-ray binary systems. In case of SGXBs, the optical companion is an OB supergiant star whereas the Be/X-ray binary systems associate with non-supergiant B-type stars which show Balmer emission lines in their spectra.

The energy spectra of accretion powered X-ray pulsars are generally described by phenomenological models consisting a power-law of photon index  $\sim 1$ , high energy cut-off (dal Fiume et al. 1998) and a Gaussian function at 6.4 keV for the presence of iron fluorescence emission. In some cases, a black-body or bremsstrahlung component is required to describe the presence of excess emission

at soft X-rays (Paul et al. 2002; Naik & Paul 2004a, 2004b; Hickox, Narayan & Kallman 2004). The broad-band X-ray spectrum of some pulsars has been described with NPEX continuum model which is an approximation of the unsaturated thermal Comptonization in hot plasma (Makishima et al. 1999). The NPEX continuum model reduces to a simple power-law with negative slope at low energies that is often used to describe the spectra of accretion powered X-ray pulsars. In case of transient Be/X-ray binary pulsars, these continuum models are marginally modified to describe the presence of absorption features at certain pulse phases. Partial covering high energy cut-off power-law model is being used to describe the broad-band spectrum of many transient pulsars (Paul & Naik 2011; Naik et al. 2011 and references therein). This model consists of two power-law continua with a common photon index but with different hydrogen-absorbing column densities. Several emission lines due to fluorescence from ions at different ionization levels and broad absorption like features due to the cyclotron resonance scattering are often seen in the pulsar spectrum. The magnetic field strength  $B$  and the cyclotron resonance energy  $E_a$  are related through the relation  $E_a = 11.6 B_{12} (1 + z_g)^{-1}$  (keV), where  $z_g$  is gravitational red-shift and  $B_{12}$  is magnetic field strength in units of  $10^{12}$  Gauss. Detection of CRSF in the spectrum, therefore, provides the direct measurement of the strength of the pulsar magnetic field. The CRSFs have been detected in the spectrum of about 19 X-ray pulsars (Coburn et al. 2002; Staubert et al. 2003; Pottschmidt et al. 2012) using data from several X-ray observatories. The harmonics of fundamental cyclotron absorption line are also detected in some pulsars (Nakajima et al. 2006; Orlandini et al. 2012).

The HMXB pulsar 4U 1909+07 was discovered with *Uhuru* satellite and mentioned as 3U 1912+07 in 3rd

<sup>1</sup> Astronomy & Astrophysics Division, Physical Research Laboratory, Ahmedabad - 380009, India. *gaurava@prl.res.in*

<sup>2</sup> Raman Research Institute, Sadashivnagar, C. V. Raman Avenue, Bangalore 560080, India

*Uhuru* catalogue (Giacconi et al. 1974). The position of the pulsar was refined and the source was renamed as 4U 1909+07 in 4th catalogue (Forman et al. 1978). The presence of many other sources in the intensity range of 2-12 mCrab and 2-10 keV energy range was reported at nearby co-ordinates of 4U 1909+07 through observations with different missions such as *OSO 7*, *Ariel 5*, *HEAO - 1*, *EXOSAT*. Wen et al. (2000) recognized that all the sources such as 4U 1909+07, 3A 1907+074, 1H 1907+074, GPS 1908+075, 1E 1908.4+0730 and X1908+075 reported through various surveys are same in uncertainty of  $1'$ . The orbital period of the binary system was reported to be 4.4 days using *Rossi X - Ray Timing Explorer (RXTE)* All-Sky Monitor (ASM) data (Wen et al. 2000). Using *RXTE* Proportional Counter Array (PCA) observations of 4U 1909+07, pulsations of 605 s were detected in the X-ray flux (Levine et al. 2004). The orbital inclination, orbital separation and mass of the companion star were estimated to be in the ranges of  $38^\circ$ – $72^\circ$ , 60–80 lt-s and 9–31  $M_\odot$ , respectively (Levine et al. 2004). The detection of an OB star in near-infrared within the X-ray error box of the pulsar confirmed the system to be a OB supergiant-neutron star HMXB (Morel & Grosdidier 2005). The distance of the binary system was estimated to be  $\sim 7$  kpc (Morel & Grosdidier 2005). *RXTE* and *INTEGRAL* observations of the pulsar showed that 605 s pulsation in the X-ray flux is not stable, rather it changes erratically on time scales of years (Fürst et al. 2011). The pulse profile was found to be strongly energy dependent. The phase averaged spectrum, obtained from above observations, were well described by a power-law with high energy cut-off continuum model along with a black-body component (Fürst et al. 2011). Fürst et al. (2012) also analyzed data from *Suzaku* observation of the pulsar and described the spectrum using same model as was used in case of their earlier work. In both cases, there was no detection of CRSF in the pulsar spectrum. Data from *Suzaku* observation was used in later case, the high energy data was truncated at 40 keV in the spectral fitting. However, using the same dataset up to high energy ranges, we detected an absorption like feature at  $\sim 44$  keV and interpret as possible CRSF in the pulsar spectrum. The details of analysis and results obtain are described in the following sections.

## 2. OBSERVATION AND ANALYSIS

The HMXB pulsar 4U 1909+07 was observed with *Suzaku* on 2010 November 2-3. We used the publicly available archival data of processing version 2.5.16.28 in present work to investigate timing and spectral properties of the pulsar. The observation was carried out at “XIS nominal” pointing position for effective exposures of  $\sim 30$  ks and  $\sim 22$  ks for X-ray Imaging Spectrometers (XIS) and Hard X-ray Detectors (HXD), respectively. XIS were operated with “normal” clock mode in “1/4 window” option. In this operation mode, the time resolution and field of view of XIS are 2 s and  $17'.8 \times 4'.4$ , respectively.

*Suzaku*, the fifth Japanese X-ray astronomy satellite, was launched by Japan Aerospace Exploration Agency (JAXA) on 2005 July 10 (Mitsuda et al. 2007). The instruments onboard *Suzaku* covers 0.2-600 keV energy range through two sets of instruments, XIS (Koyama

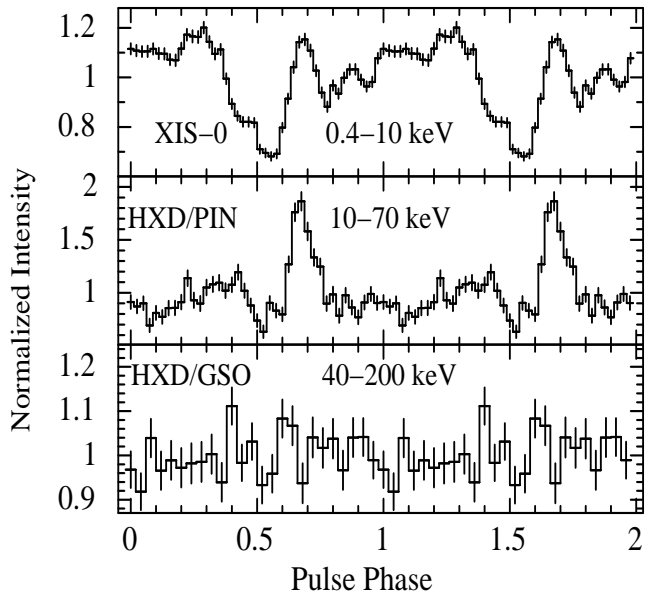


FIG. 1.— Pulse profiles of the HMXB pulsar 4U 1909+07 in 0.4-12 keV (XIS-0), 10-70 keV (HXD/PIN) and 40-200 keV (HXD/GSO) energy ranges are shown. The profiles are obtained from corresponding light curves by estimated 604.11 s pulse period of the pulsar. The errors shown in the figure are estimated for  $1\sigma$  confidence level. Two pulses are shown for clarity.

et al. 2007) and HXD (Takahashi et al. 2007). XISs are imaging CCD cameras which are located at the focal plane of X-ray telescopes (XRTs). Among the four XISs, XIS-0, XIS-2 and XIS-3 are front illuminated (FI) whereas XIS-1 is back illuminated (BI). In full window mode, the effective area of XIS is  $340 \text{ cm}^2$  for FI and  $390 \text{ cm}^2$  for BI at 1.5 keV. Due to large charge leakage in the imaging region, XIS-2 is no more operational since 2007 September. The non-imaging detector HXD consists of two types of instruments such as silicon PIN diodes covering 10–70 keV energy range and GSO crystal scintillator covering 30–600 keV energy range. The effective area of PIN is  $145 \text{ cm}^2$  at 15 keV and for GSO is  $315 \text{ cm}^2$  at 100 keV. Field of view (FoV) of XIS and PIN are  $18' \times 18'$  and  $34' \times 34'$  in open window mode, respectively. GSO has same FoV as PIN up to 100 keV. As XIS-2 is no more operational, data from other 3 XISs, PIN and GSO are used in the present analysis.

For analysis, we used HEASoft software package (version 6.12). Calibration database (CALDB) files, released on 2012 February 10 (for XIS) and 2011 September 13 (for HXD) by the instrument teams are used for data reduction. The unfiltered event files are reprocessed using ‘aepipeline’ package of FTOOLS. These reprocessed cleaned event files are used for further analysis. The arrival times of X-ray photons were converted to same at the solar system barycenter by applying “aebarycen” task of FTOOLS on the reprocessed cleaned event files of XIS, PIN and GSO. Source light curves and spectra were accumulated from XIS reprocessed cleaned event data by selecting a circular region of  $3'$  diameter around the central X-ray source. The XIS background spectra were extracted from the same event files by selecting circular regions away from the source position. By using ‘xismfgen’ and ‘xissimarfgen’ tasks of FTOOLS, the response files and effective area files for each XIS were generated for spectral fitting. Using reprocessed and cleaned HXD

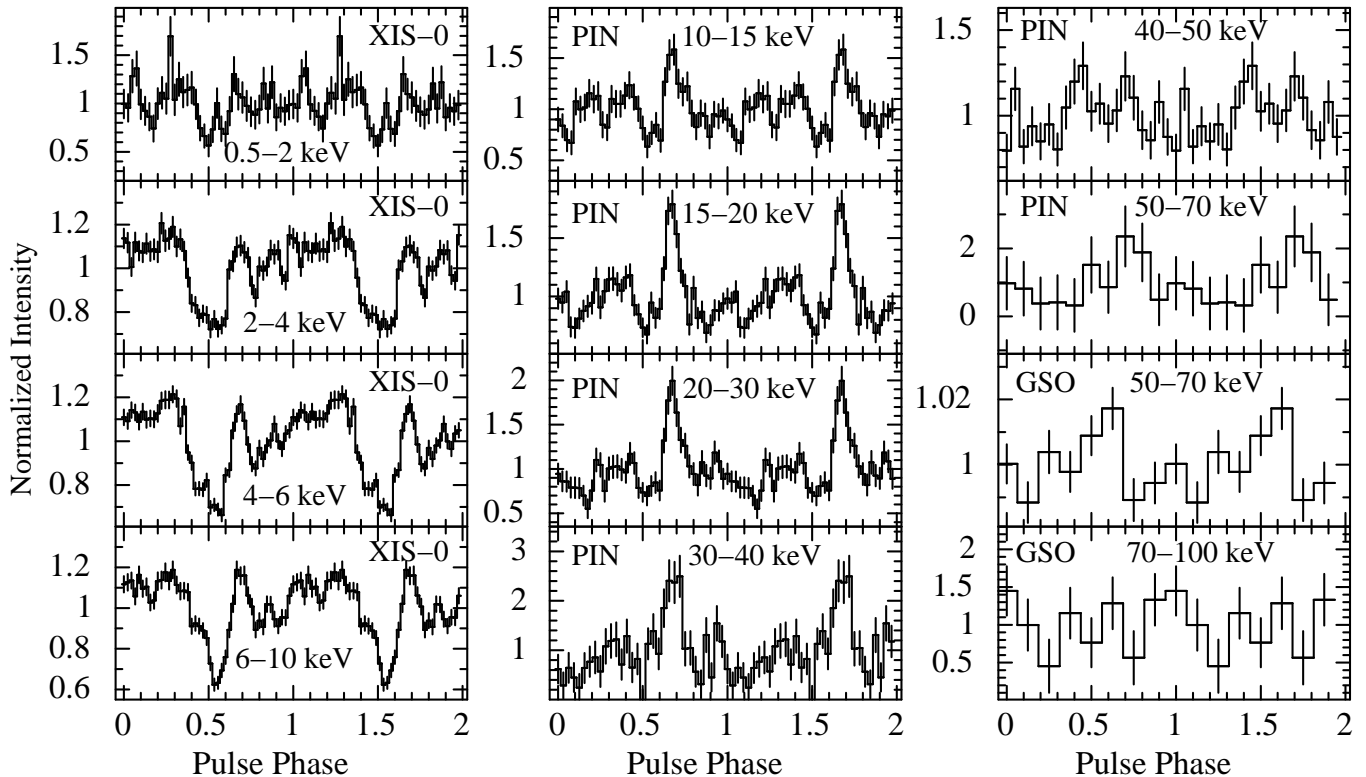


FIG. 2.— The energy resolve pulse profile of 4U 1909+07 at different energy bands obtained from XIS-0, HXD/PIN and HXD/GSO data. The evolution of pulse profile from complex shape in soft X-ray energy ranges to a single-peaked profile up to  $\sim 40$  keV can be clearly seen. The pulsation in GSO can be seen up to  $\sim 70$  keV.

data, light curves and spectra were accumulated by using the task “XSELECT” of FTOOLS. Simulated background event data (provided by the instrument teams) were used to estimate HXD/PIN and HXD/GSO background for 4U 1909+07 observation. The response files released on 2010 July (for HXD/PIN) and 2010 May (for HXD/GSO) were used for spectral analysis. Additional effective area file, released on 2010 May, was used for HXD/GSO.

### 3. RESULTS AND DISCUSSION

#### 3.1. Timing Analysis

As described above, source light curves with time resolutions of 2 s, 1 s, and 1 s were extracted from barycenter corrected XIS, HXD/PIN and HXD/GSO reprocessed event data. The orbital period of the binary system is small (4.4 days) and *Suzaku* observation of the pulsar was spanned over a significant part of the binary orbit, it is possible that the X-ray pulsations get smeared. To neutralize the effect of orbital motion on the X-ray pulsations, the photon arrival times in each of the light curves were corrected for the binary motion by using the ephemeris give by Levine et al. (2004). The orbital motion and barycenter corrected light curves were used for timing studies of the pulsar. By applying pulse folding and  $\chi^2$  maximization technique, the pulse period of the pulsar was estimated to be  $604.11 \pm 0.14$  s for XIS-0 and  $604.08 \pm 0.13$  s for HXD/PIN. The pulse periods of 604.11 s estimated from the XIS light-curve was used to generate pulse profiles of the pulsar in 0.4-12 keV, 10-70 keV and 40-200 keV energy ranges by using background subtracted XIS, HXD/PIN and HXD/GSO light curves, respectively. The corresponding pulse profiles are shown

in Figure 1. From the figure, it is seen that the pulse profiles are strongly energy dependent. In soft X-rays (top panel of the figure), the shape of the profile is found to be complex because of the presence of dip like features whereas it becomes a single peaked profile in 10-70 keV (HXD/PIN) energy range (middle panel). The pulsations are either absent or marginal in 40-200 keV (HXD/GSO) energy range (bottom panel). To investigate the evolution of pulse profile with energy, several energy resolved light curves were extracted from barycenter corrected XIS, HXD/PIN and HXD/GSO event data. Orbital correction was applied to all the light curves before generating the pulse profiles. The corresponding energy resolved pulse profiles are shown in Figure 2. The evolution of pulse profile from a complex shape at soft X-rays to a single-peaked profile up to  $\sim 70$  keV can be clearly seen in the Figure 2. It can be seen that 604.11 s pulsation is present in GSO light curves up to 70 keV energy range beyond which it is absent.

Pulse profiles of the HMXB pulsar 4U 1909+07 is strongly depends on energy. At low energies ( $\leq 10$  keV), the shape of the profile is found to be complex because of the presence of several dip like structures. These structures disappear at high energies making the pulse profile single-peaked in 10-70 keV energy range beyond which the pulsations were absent in the pulsar. Energy dependent dips or dip-like features in the pulse profile are seen in many accretion powered X-ray pulsars such as 4U 0115+63 (Tsygankov et al. 2007), A 0535+262 (Naik et al. 2008), 1A 1118-61 (Maitra et al. 2012 and references therein), GRO J1008-57 (Naik et al. 2011), EXO 2030+375 (Naik et al. 2013) etc. Detailed pulse phase resolved spectral analysis of many HMXB pulsars

such as GRO J1008-57 (Naik et al. 2011), 1A 1118-61 (Devasia et al. 2011a; Maitra et al. 2012), GX 304-1 (Devasia et al. 2011b), EXO 2030+375 (Naik et al. 2013) etc. showed complex pulse profile structure which were interpreted as due to the presence of an additional stream of matter at certain pulse phases which are phase-locked to the neutron star. Absorption of soft X-ray photons by the additional matter in narrow streams causes dips or dip like features in the pulse profiles.

### 3.2. Spectral Analysis

The pulse phase averaged spectral analysis of 4U 1909+07 was performed using spectra accumulated from XIS-0, XIS-1, XIS-3, PIN and GSO detectors. The corresponding background spectra and response files were obtained as described above. Spectra from both FI CCDs (XIS-0 and XIS-3) and corresponding background spectra and response files were merged together by applying the task ‘addascaspec’. Simultaneous spectral fitting was carried out by using spectrum, background and response data files of merged FI CCDs (0.8-10 keV), XIS-1 (0.8-10 keV), HXD/PIN (12-70 keV) and HXD/GSO (40-100 keV) with the software package XSPEC v12.7. Because of the presence of known artificial structures in XIS energy spectra at around the Si and Au edge, data in 1.7-1.9 keV and 2.2-2.4 keV energy ranges were ignored from spectral fitting. XIS spectra were re-binned by a factor of 8 from 0.8 keV to 2 keV and by a factor of 6 from 2 keV to 10 keV. HXD/PIN spectrum was re-binned by a factor of 2 from 25 keV to 40 keV and by a factor of 6 from 40 keV to 70 keV. The binning of GSO spectrum was done as suggested by the instrument team. All spectral model parameters except the relative instrument normalizations were tied together in the spectral fitting. We attempted to fit the broad-band continuum spectrum of the pulsar with (i) a simple power-law model, (ii) a high energy cut-off power-law model, (iii) the NPEX model and (iv) Comptonization continuum model (Sunyaev & Titarchuk 1985). Partial covering absorption component *pcfabs* was also applied to above continuum models in spectral fittings. Apart from these, additional components such as photoelectric absorption, Gaussian function for iron emission line, a black-body component for soft X-ray excess were needed to describe the continuum spectrum. All these models were reasonably well fitted up to  $\sim 40$  keV beyond which significant anomaly in residuals was noticed in the spectral fitting. We tried to obtain a suitable model that describes the broad-band spectrum of the pulsar in 0.8-100 keV energy range. While fitting XIS, HXD/PIN and HXD/GSO spectra simultaneously, we noticed that the relative normalization for HXD/GSO detector was high ( $\geq 2$ ) compared to XIS and HXD/PIN for all above continuum models. The relative normalizations for HXD/PIN and HXD/GSO should be same or comparable according to the HXD calibration. Apart from high value of relative instrument normalization for HXD/GSO, the spectrum beyond 100 keV also showed patterns similar to the modeled GSO background spectrum. As the pulsar is very weak in hard X-rays and there is background-like pattern in 100-150 keV source spectrum after background subtraction, it is likely that the HXD/GSO background is underestimated for this *Suzaku* observation. Considering this, we did not use the HXD/GSO spectrum in

spectral fitting and fitted 0.8-70 keV spectrum extracted from XIS and HXD/PIN data by using above models.

The partial covering power-law continuum model with iron emission line and a black-body component of temperature  $\sim 3$  keV fitted the pulsar spectrum well. A black-body component with high temperature as  $\sim 3$  keV is unusual in case of accretion powered X-ray pulsars. The addition of high energy cut-off to the partial covering power-law model fitted data well with the black-body temperature of  $\sim 0.2$  keV. The parameters obtained by fitting the partial covering high energy cut-off power-law model to the spectrum are in good agreement with Table 2 of Fürst et al. (2012). However, the partial covering NPEX continuum model with iron line and black-body component described the spectrum better yielding an acceptable black-body temperature of 0.2 keV. An absorption like feature was seen in pulsar spectrum and in the residuals at  $\sim 44$  keV that allowed to add a CRSF component in the spectral model. The addition of CRSF component to above continuum models improved  $\chi^2$  values for each model (as given in Table 1). The count rate spectra of the pulsar 4U 1909+07 are shown in Figure 3 (for partial covering power-law model), Figure 4 (for partial covering high energy cut-off power-law model) and Figure 5 (for partial covering NPEX model) along with the model components (top panels). The middle panels in above three figures show the residuals to the fitted models without the CRSF whereas the bottom panels show the residuals to the best-fitting model using the CRSF component in the spectral models. The presence of an absorption feature at  $\sim 44$  keV can be clearly seen in the middle panels of all figures.

To test the statistical significance of the  $\chi^2$  improvement due to the addition of the CRSF component, we performed an F-test. In case of emission line features (additive components in *XSPEC*), the *F*-test routine incorporated in *XSPEC* package should be the best suited to perform the significance test (though care should be taken while using this - see Protassov et al. 2002). However, in case of multiplicative components such as CRSF, the *F*-test in *XSPEC* is inappropriate for performing the null hypothesis test. The *F*-test in *XSPEC* is based on the assumption that the inclusion of the new component does not alter the continuum. This is true if the component is added to the continuum model, whereas this is not correct if the component is multiplied by the continuum. Therefore, we used a different *F*-test, as described in Press et al. (2007), to test the statistical significance of the CRSF component in the spectrum of 4U 1909+07 (see e.g. Orlandini et al. 2012). The *F*-test routine is available in *IDL* package (named as *mpftest*<sup>3</sup>) and was used for significance test of multiplicative components such as CRSF or Gaussian absorption features (Decesar et al. 2013). The probability of chance improvement (PCI) is evaluated for each of the three models used to fit the pulsar spectrum without and with CRSF component. The estimated PCI values after addition of CRSF component to the (i) partial covering power-law model with black-body, (ii) partial covering high-energy cutoff power-law model with black-body and (iii) partial covering NPEX model with black-body are found to be 37%, 51% and 47%, respectively. Considering the high value of PCI for all three models, the CRSF is found to be not statistically significant. But the residuals shown

<sup>3</sup> <http://www.physics.wisc.edu/~craigm/idl/down/mpftest.pro>

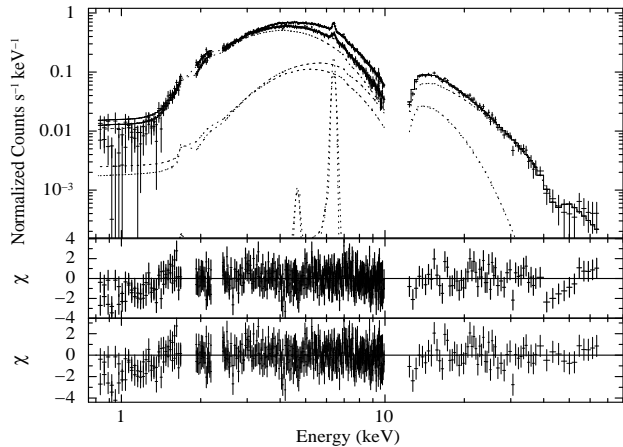


FIG. 3.— Energy spectrum of 4U 1909+07 obtained with XIS and HXD/PIN detectors of *Suzaku* observation, along with the fitted model comprising a partial covering power-law continuum model along with a black-body component, a narrow iron line emission, and a CRSF. The middle and bottom panels show the contributions of the residuals to  $\chi^2$  for each energy bin for the partial covering power-law continuum model without and with CRSF component in the model, respectively.

in the middle panels of Figures 3, 4 & 5 clearly show an absorption-like feature at  $\sim 44$  keV. It may be noted that the goodness-of-fit estimator chosen here to assess the statistical significance of the CRSF (the  $\chi^2$ ) is not the best suited as it does not take into account the “shape” of the residuals. Considering the identical distribution of residuals around 40 keV (middle panels of Figures 3, 4 & 5, we applied run-test (also called Wald-Wolfowitz test) on the residuals obtained from the spectral fitting by using above three continuum models. IDL routine for run-test<sup>4</sup> was used to derive the null hypothesis of the randomness in the residuals of spectral fitting in 37-65 keV energy range. It was found that the number of data points used for the run-test in 37-65 keV energy range are 12 (6 points below zero and 6 points above zero), 13 (4 points below zero and 9 points above zero) and 13 (6 points below zero and 7 points above zero) for partial covering power-law, partial covering high-energy cutoff and partial covering NPEX continuum models, respectively. The probability for getting 3 runs in above energy range was estimated to be 0.8%, 0.7% and 0.5%, respectively. Marginal difference in the values of probability is because of the use of different continuum models that can affect the residuals in the spectral fitting. The computed probability of  $\leq 1\%$  for all three continuum models reject the hypothesis of random sampling of the detected absorption feature in the pulsar spectrum. Among the three continuum models, it is found that the NPEX continuum model with black-body, a Gaussian function and a CRSF feature at  $\sim 44$  keV yields the best fit to 0.8-70 keV data. The presence of an absorption feature at  $\sim 44$  keV in the residuals of all the models suggest that the CRSF is indeed required in the spectral fitting. The best-fit spectral parameters obtained by using three different continuum models along with additional components are given in Table 1. It can be seen from the table that addition of a CRSF at  $\sim 44$  keV improved the spectral fitting in all cases.

The same *Suzaku* observation was analyzed, although with the ISIS package, by Fürst et al. (2012). These authors did not use HXD/GSO data because of possible contamination from the nearby source GRS 1915+105, and therefore performed their spectral analysis in the 1-40 keV energy range. Considering the earlier result, the possible CRSF

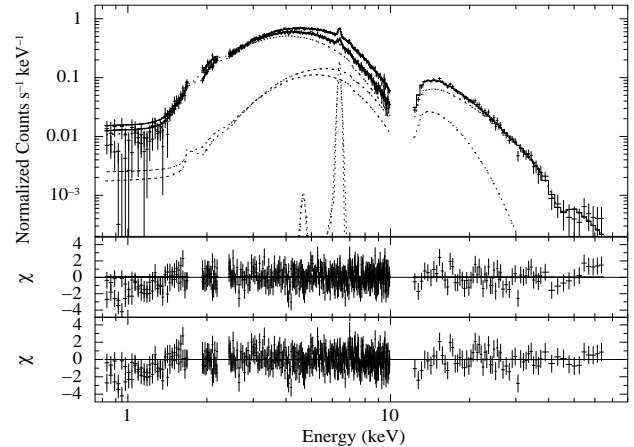


FIG. 4.— Energy spectrum of 4U 1909+07 obtained with XIS and HXD/PIN detectors of *Suzaku* observation, along with the fitted model comprising a partial covering high energy cut-off power-law continuum model along with a black-body component, a narrow iron line emission, and a CRSF. The middle and bottom panels show the contributions of the residuals to  $\chi^2$  for each energy bin for the partial covering power-law continuum model without and with CRSF component in the model, respectively.

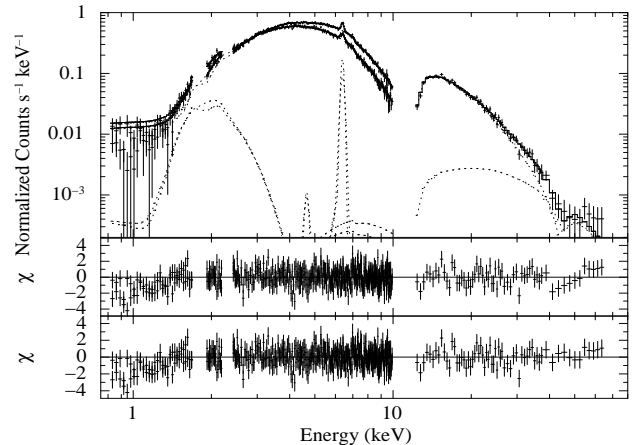


FIG. 5.— Energy spectrum of 4U 1909+07 obtained with XIS and HXD/PIN detectors of *Suzaku* observation, along with the best-fit model comprising a partial covering NPEX continuum model along with a black-body component, a narrow iron line emission, and a CRSF. The middle and bottom panels show the contributions of the residuals to  $\chi^2$  for each energy bin for the partial covering NPEX continuum model without and with CRSF component in the model, respectively.

feature at  $\sim 44$  keV was carefully examined by different approaches. As the pulsar is weak in hard X-ray energy ranges, we tried to establish that the observed photons in the spectrum beyond  $\sim 40$  keV are not affected by detector energy response uncertainties. We extracted pulsar light curves in 10-40 keV, 40-50 keV and 50-70 keV energy ranges from HXD/PIN and HXD/GSO reprocessed event data. Corresponding background light curves were also extracted from the simulated background event data (as described in the previous section). The background subtracted and orbital corrected light curves in above energy ranges were used to generate power density spectra. The energy resolved power density spectra of 4U 1909+07, as shown in Figure 6, show additional power (peaks) at  $\sim 1.65$  mHz (the spin frequency of the pulsar) in 10-40 keV (top panel), 40-50 keV (second panel) and 50-70 keV (third and fourth panels) energy ranges. The power density spectra shown in top three panels were extracted from corresponding light curves obtained from

<sup>4</sup> <http://www.astro.washington.edu/docs/idl/cgi-bin/getpro/library/html?RTEST>

TABLE 1

BEST-FIT PARAMETERS OF THE PHASE-AVERAGED SPECTRA FOR 4U 1909+07 OF *Suzaku* OBSERVATION WITH  $1\sigma$  ERRORS. MODEL-1 : PARTIAL COVERING POWER-LAW MODEL WITH BLACK-BODY AND GAUSSIAN COMPONENTS, MODEL-2 : PARTIAL COVERING POWER-LAW MODEL WITH BLACK-BODY, GAUSSIAN COMPONENTS AND CYCLOTRON LINE. MODEL-3 : PARTIAL COVERING HIGH ENERGY CUT-OFF POWER-LAW MODEL WITH BLACK-BODY AND GAUSSIAN COMPONENTS, MODEL-4 : PARTIAL COVERING HIGH ENERGY CUT-OFF POWER-LAW MODEL WITH BLACK-BODY, GAUSSIAN COMPONENTS AND CYCLOTRON LINE. MODEL-5 : PARTIAL COVERING NPEX MODEL WITH BLACK-BODY AND GAUSSIAN COMPONENTS, MODEL-6 : PARTIAL COVERING NPEX MODEL WITH BLACK-BODY, GAUSSIAN COMPONENTS AND CYCLOTRON LINE

Parameter	Value					
	Model-1	Model-2	Model-3	Model-4	Model-5	Model-6
$N_{H1}$ ( $10^{22}$ atoms $\text{cm}^{-2}$ )	$6.16 \pm 0.17$	$5.95 \pm 0.19$	$7.50 \pm 0.21$	$7.53 \pm 0.25$	$7.09 \pm 0.20$	$7.05 \pm 0.19$
$N_{H2}$ ( $10^{22}$ atoms $\text{cm}^{-2}$ )	$9.71 \pm 0.95$	$8.20 \pm 1.28$	$32.19 \pm 8.20$	$34.01 \pm 7.82$	$38.78 \pm 7.89$	$39.71 \pm 7.90$
Covering Fraction	$0.52 \pm 0.03$	$0.47 \pm 0.05$	$0.18 \pm 0.04$	$0.18 \pm 0.03$	$0.19 \pm 0.03$	$0.20 \pm 0.03$
$kT_{BB}$ (keV)	$3.38 \pm 0.21$	$2.71 \pm 0.23$	$0.19 \pm 0.01$	$0.19 \pm 0.01$	$0.20 \pm 0.01$	$0.20 \pm 0.01$
Norm. <sup>a</sup> of $kT_{BB}$ ( $10^{-3}$ )	$1.50 \pm 0.14$	$1.18 \pm 0.18$	$10.59 \pm 3.25$	$11.07 \pm 3.10$	$5.65 \pm 1.70$	$5.27 \pm 1.82$
Iron line Energy (keV)	$6.39 \pm 0.01$	$6.39 \pm 0.01$	$6.39 \pm 0.01$	$6.39 \pm 0.01$	$6.39 \pm 0.01$	$6.39 \pm 0.01$
Iron line width (keV)	$0.01 \pm 0.01$	$0.01 \pm 0.01$	$0.01 \pm 0.01$	$0.01 \pm 0.01$	$0.01 \pm 0.01$	$0.01 \pm 0.01$
Iron line eq. width (eV)	$73 \pm 3$	$72 \pm 3$	$68 \pm 3$	$68 \pm 3$	$69 \pm 3$	$68 \pm 3$
Power-law index	$1.91 \pm 0.03$	$1.77 \pm 0.05$	$1.43 \pm 0.05$	$1.44 \pm 0.04$	$1.05 \pm 0.06$	$1.01 \pm 0.07$
Norm. <sup>b</sup> of Power-law ( $10^{-2}$ )	$7.40 \pm 0.51$	$5.36 \pm 0.71$	$4.16 \pm 0.50$	$4.26 \pm 0.52$		
High energy cut-off (keV)			$7.34 \pm 0.28$	$7.37 \pm 0.16$	$13.98 \pm 1.77$	$12.78 \pm 1.58$
Folding energy (keV)			$23.42 \pm 1.51$	$24.23 \pm 1.10$		
Cyclotron line $E_a$ (keV)		$43.75 \pm 1.51$		$43.10 \pm 2.09$		$43.85 \pm 1.58$
Width of cyclotron line (keV)		$4.72 \pm 2.58$		$1.0^{+2.5}_{-1.0}$		$2.04 \pm 2.02$
Depth of cyclotron line		$1.25 \pm 0.50$		$1.01 \pm 0.83$		$1.57 \pm 0.89$
Flux <sup>c</sup> (in 1-10 keV range)	$1.51 \pm 0.10$	$1.51 \pm 0.03$	$1.51 \pm 0.18$	$1.51 \pm 0.16$	$1.51 \pm 0.15$	$1.51 \pm 0.14$
Flux <sup>c</sup> (in 10-70 keV range)	$4.22 \pm 0.29$	$4.14 \pm 0.40$	$3.76 \pm 0.42$	$3.76 \pm 0.38$	$3.94 \pm 0.69$	$4.01 \pm 0.75$
$C_{XIS-03}/C_{XIS-1}/C_{PIN}$	$1.0/0.94/1.11$	$1.0/0.94/1.22$	$1.0/0.94/1.18$	$1.0/0.94/1.17$	$1.0/0.94/1.13$	$1.0/0.94/1.13$
$\chi^2$ (dofs)	609 (489)	587 (486)	576 (487)	573 (484)	578 (487)	570 (484)

$N_{H1}$  = Equivalent hydrogen column density,  $N_{H2}$  = Additional hydrogen column density, <sup>a</sup> : in units of  $10^{39}$  erg  $\text{s}^{-1}$   $(d/10 \text{ kpc})^{-2}$  where  $d$  is the distance to the source, <sup>b</sup> : photons  $\text{keV}^{-1} \text{cm}^{-2} \text{s}^{-1}$  at 1 keV, <sup>c</sup> : Absorption uncorrected flux (in units of  $10^{-10}$  ergs  $\text{cm}^{-2} \text{s}^{-1}$ ).

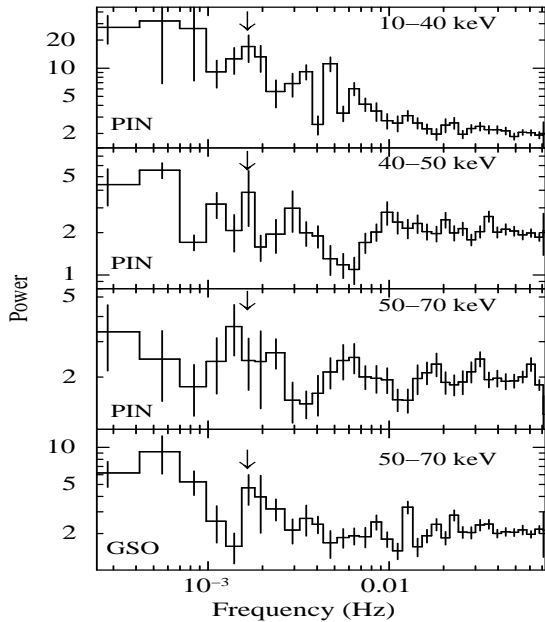


FIG. 6.— The power density spectra of the HMXB pulsar 4U 1909+07 in 10-40 keV (top panel), 40-50 keV (second panel) and 50-70 keV (third and fourth panels) ranges are shown. Background subtracted and orbital corrected HXD/PIN and HXD/GSO light curves were used to generate power density spectra in each energy range. The arrows indicate the spin period of the pulsar. Additional power can be seen at  $\sim 1.65$  mHz (spin frequency of the pulsar) in all panels

HXD/PIN data where as the one shown in bottom panel was extracted from HXD/GSO data. The presence of additional power at  $\sim 1.65$  mHz in the power density spectra in 40-50 keV and 50-70 keV confirms that photons beyond 40 keV in the spectrum are not associated with any energy response uncertainties.

To establish the absorption like feature seen at  $\sim 44$  keV in the pulsar spectrum as CRSF, we evaluated the energy spectra of the pulsar 4U 1909+07 in a model-independent manner. We attempted to normalize the pulsar spectrum with that of Crab Nebula, the spectrum of which is a featureless power-law with a photon index of  $\sim 2.1$ . The normalization (Crab ratio) has the advantage of minimizing the effects due to the detector response and the uncertainties in the energy response. To generate Crab ratio, we used a Crab observation with *Suzaku* (on 2010 April 5) that is nearest to the observation of the pulsar 4U 1909+07. Data reduction and background estimation for HXD/PIN data of Crab observation were done as described above and the Crab ratio was obtained to investigate the presence of the absorption feature in the pulsar spectrum. The resulting Crab ratio in 12-70 keV energy range is shown in Figure 7. The presence of the absorption feature at  $\sim 44$  keV, as was seen in the spectral fitting (middle panels of Figures 3, 4 & 5, can be clearly seen in the figure. It should be noted here that the shape of this CRSF-like feature in Crab ratio was very similar to that seen in the middle panels of above figures. In order to evaluate the statistical significance of the absorption feature, we performed a run-test on the Crab-ratio data. It was found that in 37-65 keV energy range in Crab ratio, there are 13 data points with 3 runs in which 7 points are above zero and 6 points are below zero. The probability of obtaining 3 runs is only  $\sim 1\%$ . This result, together with the results obtained from the analysis on the spectral residuals, strongly supports the genuine presence of absorption feature in the Crab ratio at  $\sim 44$  keV. It confirms the presence of CRSF at  $\sim 44$  keV in the HMXB pulsar 4U 1909+07.

#### 4. CONCLUSION

In this work, we have studied timing and spectral properties of the HMXB pulsar 4U 1909+07 using data from *Suzaku* observation. The pulse profiles are strongly depend on energy and evolve from complex shape at lower energy to single peaked profile at higher energy. Broad-band spectroscopy

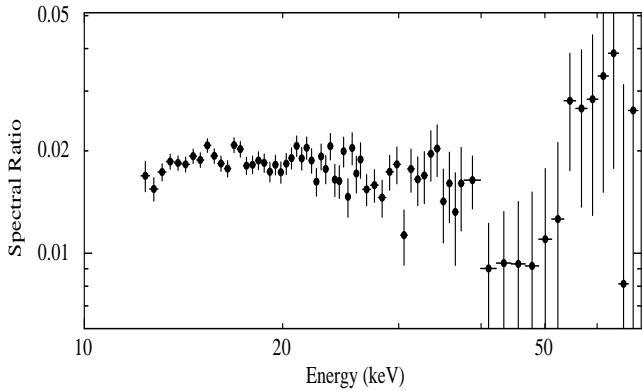


FIG. 7.— Ratio between the background subtracted HXD/PIN spectra of the HMXB pulsar 4U 1909+07 and Crab Nebula. The absorption feature at  $\sim 44$  keV is clearly seen.

of the HMXB pulsar 4U 1909+07 in 1-70 keV energy range is reported for the first time here. Though the pulsar is very weak in hard X-rays, the high sensitivity of the HXD onboard *Suzaku* helped in performing phase-averaged spectroscopy up to as high as 70 keV. The energy spectrum of X-ray pulsar is well described by partial covering NPEX model with blackbody component. For the first time, we report the possible detection of CRSF at  $\sim 44$  keV in this pulsar. Based on this detection, the magnetic field strength at the neutron star surface is estimated to be  $\sim 3.8 \times 10^{12}$  Gauss. It is seen that the

values of CRSF detected in accretion powered X-ray pulsars follow a continuum distribution starting from as low as  $\sim 11$  keV for 4U 0115+634 (Nakajima et al. 2006) to as high as  $\sim 76$  keV for GRO J1008-57 (Yamamoto et al. 2013). Nevertheless a CRSF at  $\sim 100$  keV is reported in LMC X-4 (La Barbera et al. 2001), it is yet to be confirmed. Considering the confirmed values of CRSF in X-ray pulsars, the CRSF detected in the pulsar 4U 1909+07 in present work falls in the higher side. It is to be noted that we report the detection of CRSF at  $\sim 44$  keV in the spectrum of 4U 1909+07, obtained from a  $\sim 22$  ks of exposure with HXD. *Suzaku* observation with long exposure is required to confirm the presence of the absorption feature in this pulsar. The LAXPC instrument of the upcoming *Astrosat* mission will also provide a very good opportunity to establish the CRSF feature in the slow HMXB pulsar 4U 1909+07.

#### ACKNOWLEDGMENTS

The authors would like to thank the anonymous referee for his/her constructive comments and suggestions that improved the contents of the paper. The research work at Physical Research Laboratory is funded by the Department of Space, Government of India. The authors would like to thank all the members of *Suzaku* for their contributions in the instrument preparation, spacecraft operation, software development, and in-orbit instrumental calibration. This research has made use of data obtained through HEASARC Online Service, provided by NASA/GSFC, in support of NASA High Energy Astrophysics Programs.

#### REFERENCES

- Coburn W., et al. 2002, ApJ, 580, 394  
 dal Fiume D., et al. 1998, A&A, 329, L41  
 Decesar M. E., Boyd P. T., Pottschmidt K., et al. 2013, ApJ, 762, 61  
 Devasia J., James M., Paul B., Indulekha K., 2011a, MNRAS, 414, 1023  
 Devasia J., James M., Paul B., Indulekha K., 2011b, MNRAS, 417, 348  
 Forman W., et al. 1978, A&AS, 38, 357  
 Fürst F., et al. 2011, A&A, 525, 73  
 Fürst F., et al. 2012, A&A, 547, 2  
 Giacconi R., et al. 1971, ApJ, 167, L67  
 Giacconi R., Murray S., Gursky H., et al. 1974, A&AS 27, 37  
 Hickox R. C., Narayan R., Kallman T. R., 2004, ApJ, 614, 881  
 Koyama K., et al. 2007, PASJ, 59, 23  
 La Barbera A., Burderi L., Di Salvo T., Iaria R., Robba N. R., 2001, ApJ, 553, 375  
 Levine A. M., Rappaport S., Remillard R., Savcheva A., 2004, ApJ, 617, 1284  
 Maitra C., Paul B., Naik S., 2012, MNRAS, 420, 2307  
 Makishima K., Mihara T., Nagase F., Tanaka Y., 1999, ApJ, 525, 978  
 Mitsuda K., et al. 2007, PASJ, 59, 1  
 Morel T., Grosdidier Y., 2005, MNRAS, 356, 665  
 Naik S., Paul B., 2004a, ApJ, 600, 351  
 Naik S., Paul B., 2004b, A&A, 418, 655  
 Naik S., et al. 2008, ApJ, 672, 516  
 Naik S., Paul B., Kachhara C., Vadawale S. V., 2011, MNRAS, 413, 241  
 Naik S., Maitra C., Jaisawal G. K., Paul B., 2013, ApJ, 764, 158  
 Nakajima, M., Mihara, T., Makishima, K., Niko, H., 2006, ApJ, 646, 1125  
 Orlandini M., Frontera F., Masetti N., et al. 2012, ApJ, 748, 86  
 Paul B., Nagase F., Endo T., Dotani T., Yokogawa J., Nishiuchi M., 2002, ApJ, 579, 411  
 Paul B., Naik, S., 2011, BASI, 39, 429  
 Pottschmidt K., et al. 2012, AIPC, 1427, 60  
 Press W. H., Teukolsky S. A., Vetterling W. T., & Flannery, B. P. 2007, Numerical Recipes: The Art of Scientific Computing (Cambridge: Cambridge Univ. Press), 730  
 Protassov R., et al. 2002, ApJ, 571, 545  
 Reynolds A. P.; Quaintrell H., Still M. D., et al. 1997, MNRAS, 288, 43  
 Staubert R., 2003, ChJAS, 3, 270  
 Sunyaev & Titarchuk, 1985, A&A, 143, 374  
 Takahashi T., et al. 2007, PASJ, 59, 35  
 Tsygankov S. S., Lutovinov A. A., Churazov E. M., Sunyaev, R. A., 2007, Astronomy Letters, 33, 368  
 Yamamoto T., Mihara T., Sugizaki M., Sasano M., Makishima K., Nakajima M., 2013, Astr. Tel., 4759  
 Wen L., Remillard R. A., Bradt H. V., 2000, ApJ, 532, 1119